International Journal of Heat and Mass Transfer 139 (2019) 115–120

Contents lists available at ScienceDirect

International Journal of Heat and Mass Transfer

journal homepage: www.elsevier.com/locate/ijhmt

Technical Note

Conduction heat transfer from oblate spheroids and bispheres

Saeed Jafari Kang, Esmaeil Dehdashti, Hassan Masoud *

Department of Mechanical Engineering-Engineering Mechanics, Michigan Technological University, Houghton, MI 49931, USA

ARTICLE INFO

Article history:
Received 19 February 2019
Received in revised form 17 April 2019
Accepted 28 April 2019

Keywords:
Conduction
Laplace's equation
Oblate spheroid
Bisphere
Separation of variables

ABSTRACT

We theoretically examine heat transfer by conduction from oblate spheroidal and bispherical surfaces into a stationary, infinite medium. The surfaces are presumed to maintain a constant heat flux. Assuming steady-state condition and uniform thermal conductivity, we analytically solve Laplace's equation for the temperature distribution and discuss the challenge of dealing with the Neumann (uniform flux) versus more convenient Dirichlet (isothermal) boundary condition. The solutions are obtained in boundary-fitting coordinate systems using the method of separation of variables and eigenfunction expansion. And, exact expressions for the average Nusselt number are presented along with their approximations.

1. Introduction

In the area of heat transfer (like other fields of science and engineering), analytical solutions of elementary problems are regarded as invaluable resources that can be used to identify relevant dimensionless parameters, to obtain basic insights into the phenomena under consideration, to quickly quantify the effects of key factors, and, ultimately, to pave the way for understanding more complex problems arising in practice. The solutions can also serve as excellent benchmarks for calibrating experimental setups and validating numerical techniques. Last but not least, analytical solutions are usually used for teaching students fundamental concepts. Hence, they are educationally worthwhile, too.

Here, we present analytical solutions for the problem of steady-state conduction heat transfer in an infinite medium due to the presence of hot/cold inclusions. Specifically, two geometries for the heat source/sink are considered, namely an oblate spheroid and a pair of spheres (see Figs. 1 and 2). For both cases, a uniform heat flux is assumed to emanate from the surface of the inclusions. This boundary condition models many scenarios that appear frequently in engineering applications, such as when a surface is covered by a thin layer of electric heater [1]. The assumption of the Neumann boundary condition is the novel aspect of our study. As we shall see in Sections 2.1 and 2.2, mathematical derivations under this condition become more challenging compared to the situation where an isothermal (Dirichlet) surface condition is considered.

In what follows, we first formulate the problem mathematically and then provide a detailed description of the solutions for the two geometries of interest. Next, we discuss the results for the temperature distribution and average Nusselt number and, finally, we give a brief summary of our study.

2. Problem formulation and solutions

Consider one or more objects surrounded by an infinite medium at rest. Suppose that heat is released/absorbed from/by the surface of the objects at a constant uniform rate and that the temperature at infinity is maintained at a constant value. Of interest here is the steady-state temperature distribution in the surrounding medium assuming that the transport of heat is dominated by conduction and that the thermal conductivity is constant. Given the above conditions, the boundary-value problem governing the distribution of the temperature is

$$\begin{aligned} &\nabla^2 T = 0 \quad \text{with} \\ &-k\boldsymbol{n}\cdot\nabla T = q_s \text{ for } \boldsymbol{r}\in S_o \quad \text{and} \quad T\to T_\infty \text{ as } r\to\infty, \end{aligned} \tag{1}$$

where T represents the temperature field, k is the thermal conductivity of the medium, $\boldsymbol{n}$ is the unit vector outward normal to the surface of the objects denoted by S_o, $\boldsymbol{r}$ is the position vector with magnitude $r=|\boldsymbol{r}|$, and q_s and T_∞ are constants.

Let ℓ be a characteristic length scale of the problem. Then, upon the change of variables $\theta = k(T-T_\infty)/q_s\ell, \tilde{\boldsymbol{r}} = \boldsymbol{r}/\ell$, and $\tilde{r} = r/\ell$, Eq. (1) simplifies to the following dimensionless form:

* Corresponding author.
E-mail address: hmasoud@mtu.edu (H. Masoud).

https://doi.org/10.1016/j.ijheatmasstransfer.2019.04.138
0017-9310/

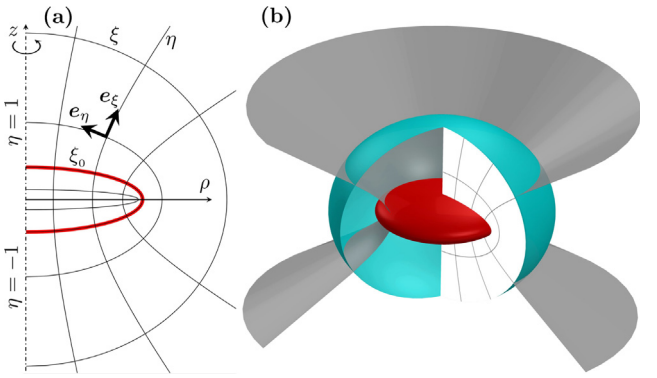

Fig. 1. (a) Oblate spheroidal coordinates in a meridian plane. The arrows show the direction of the unit vectors $\boldsymbol{e}_\xi$ and $\boldsymbol{e}_\eta$. (b) Surfaces of constant ξ and η depicted in cyan and gray, respectively. The red curve in (a) and its corresponding surface in (b) represent a hot/cold oblate spheroid that releases/absorbs heat at a constant uniform rate. (For interpretation of the references to colour in this figure legend, the reader is referred to the web version of this article.)

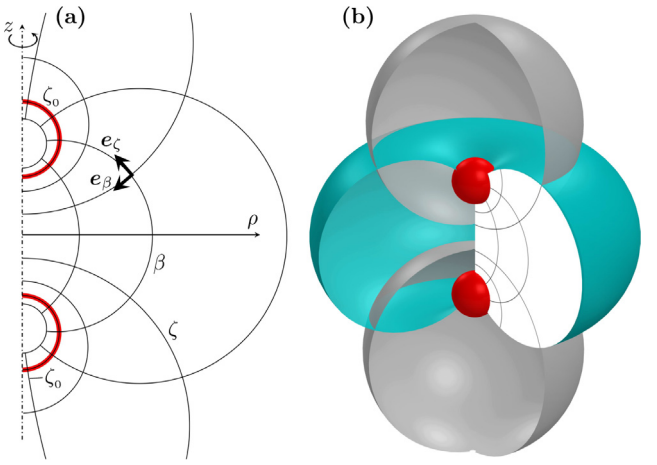

Fig. 2. (a) Bispherical coordinates in a meridian plane. The arrows show the direction of the unit vectors $\boldsymbol{e}_\zeta$ and $\boldsymbol{e}_\beta$. (b) Surfaces of constant ζ and β depicted in cyan and gray, respectively. The red curves in (a) and their corresponding surfaces in (b) represent a pair of identical hot/cold spheres that release/absorb heat at a constant uniform rate. (For interpretation of the references to colour in this figure legend, the reader is referred to the web version of this article.)

$$\nabla^2\theta = 0 \quad \text{with}$$
$$\boldsymbol{n}\cdot\nabla\theta = -1 \text{ for } \tilde{\boldsymbol{r}} \in S_o \quad \text{and} \quad \theta \to 0 \text{ as } \tilde{r} \to \infty. \tag{2}$$

One can define an average Nusselt number for this problem as

$$\mathrm{Nu} = \frac{\mathbb{S}_o}{2\pi\bar{\theta}_s}, \tag{3}$$

where $\mathbb{S}_o$ represents the dimensionless surface area of the object and $\bar{\theta}_s$ is the mean value of θ on S_o. Below, we solve Eq. (2) and calculate the average temperature for cases in which S_o represents the surface of an oblate spheroid and a pair of spheres, respectively. For each case, the solution is obtained via the method of separation of variables and eigenfunction expansion in a coordinate system that matches the boundaries of the problem.

The correctness of the derivations is independently verified by comparing the results against those obtained from the numerical solution of Eq. (2). A second-order finite volume method as implemented in *OpenFOAM* (see, e.g., [2]) is used to perform the computations. The outer boundary at infinity is modeled as a very large sphere, and 2D axisymmetric meshes concentrated around S_o are employed to discretize the physical domains.

2.1. Temperature field around an oblate spheroid

Consider an oblate spheroid of equatorial radius ℓ and aspect ratio (ratio of polar to equatorial radius) ε. Let (x, y, z) be the components of a reference Cartesian coordinate system located at the center of the spheroid such that the z axis coincides with the revolution axis of the spheroid. The coordinates are nondimentionalized by ℓ. To solve Eq. (2), we adopt an oblate spheroidal coordinate system (ξ, η, φ) defined as [3,4]

$$x/\cos\varphi = y/\sin\varphi = c\sqrt{(1+\xi^2)(1-\eta^2)}, \quad z = c\,\xi\,\eta, \tag{4}$$

where $c = \sqrt{1-\varepsilon^2}$ is the (dimensionless) radius of the focal circle and

$$0 \leqslant \xi < \infty, \quad -1 \leqslant \eta \leqslant 1, \quad 0 \leqslant \varphi < 2\pi. \tag{5}$$

The metric coefficients associated with (ξ, η, φ) are

$$h_\xi = c\sqrt{\frac{\xi^2+\eta^2}{1+\xi^2}}, \quad h_\eta = c\sqrt{\frac{\xi^2+\eta^2}{1-\eta^2}}, \quad h_\varphi = \rho = \sqrt{x^2+y^2}. \tag{6}$$

As shown in Fig. 1, the surfaces of constant ξ and η are oblate spheroids and one-sheet hyperboloids of revolution, respectively. In particular, $\xi = \xi_0 = \varepsilon/\sqrt{1-\varepsilon^2}$ represents S_o and $\xi \to \infty$ corresponds to a bounding surface at large distances.

In the orthogonal curvilinear coordinate system (ξ, η, φ), Eq. (2) takes the form of [3,4]

$$\nabla^2\theta = \frac{1}{c^2(\xi^2+\eta^2)}\left\{\frac{\partial}{\partial\xi}\left[(1+\xi^2)\frac{\partial\theta}{\partial\xi}\right] + \frac{\partial}{\partial\eta}\left[(1-\eta^2)\frac{\partial\theta}{\partial\eta}\right]\right\}$$
$$+\frac{1}{c^2(1+\xi^2)(1-\eta^2)}\frac{\partial^2\theta}{\partial\varphi^2} = 0 \quad \text{with} \tag{7}$$
$$\frac{1}{h_\xi}\frac{\partial\theta}{\partial\xi}\bigg|_{\xi=\xi_0} = -1 \quad \text{and} \quad \theta \to 0 \text{ as } \xi \to \infty.$$

Since the boundary conditions do not depend on φ, we deduce that θ is azimuthally independent, i.e., $\partial\theta/\partial\varphi = 0$. Hence, Laplcae's equation for θ reduces to

$$\frac{\partial}{\partial\xi}\left[(1+\xi^2)\frac{\partial\theta}{\partial\xi}\right] + \frac{\partial}{\partial\eta}\left[(1-\eta^2)\frac{\partial\theta}{\partial\eta}\right] = 0. \tag{8}$$

Starting with the ansatz $\theta(\xi,\eta) = \mathcal{X}(\xi)\mathcal{H}(\eta)$, where $\mathcal{X}$ and $\mathcal{H}$ are to-be-determined functions, and following the steps involved in the separation of variables technique [3,4], it can be shown that the general solution of Eq. (8) is

$$\theta = \sum_{m=0}^{\infty}\left[A_m^1 P_m(i\xi) + A_m^2 Q_m(i\xi)\right]\left[A_m^3 P_m(\eta) + A_m^4 Q_m(\eta)\right], \tag{9}$$

where m is an integer, $A_m^1, \ldots, A_m^4$ are constants, $i^2 = -1$, and P_m and Q_m are Legendre functions of the first and second kind, respectively [5]. The latter function is defined as:

$$Q_0(z) = \tfrac{1}{2}\ln\left(\tfrac{z+1}{z-1}\right),\ Q_1(z) = \tfrac{z}{2}\ln\left(\tfrac{z+1}{z-1}\right) - 1,$$
$$Q_{n+1}(z) = \tfrac{(2n+1)z\,Q_n - n\,Q_{n-1}}{n+1}$$

The function $P_m(i\xi)$ blows up as $\xi \to \infty$ for $m \neq 0$ and so does $Q_m(\eta)$ at $\eta = \pm 1$ for all m. Therefore, to keep the solution finite, we need to set $A_m^1 = 0$ for $m \neq 0$ and $A_m^4 = 0$ for all m. By demanding θ to vanish at infinity, we find that A_0^1 is zero, too, since $P_0(i\xi) = P_0(\eta) = 1$ and $Q_m(i\xi)$ decays to zero for large ξ. Thus, Eq. (9) simplifies to

$$\theta = \sum_{m=0}^{\infty} A_m\, Q_m(i\xi)\, P_m(\eta), \tag{10}$$

where the constant coefficients A_m are determined by applying the constant flux boundary condition on S_o:

$$\frac{1}{h_\xi}\frac{\partial\theta}{\partial\xi}\bigg|_{\xi=\xi_0} = \frac{i}{c}\sqrt{\frac{1+\xi_0^2}{\xi_0^2+\eta^2}}\sum_{m=0}^{\infty} A_m\, Q'_m(i\xi_0)\, P_m(\eta) = -1, \tag{11}$$

with $Q'_m(x) = \mathrm{d}Q_m(x)/\mathrm{d}x$. Note that although the gradient of θ in the direction normal to the boundary is constant, its derivative with respect to ξ (coordinate normal to the boundary) is equal to the scale factor h_ξ, which varies along the boundary. Had we been considering the constant temperature boundary condition (i.e., $\theta = 1$) at $\xi = \xi_0$, we would have been dealing with a significantly simpler situation where θ would have been also independent of η and Eq. (8) would have further reduced to an ordinary differential equation with the solution (see, e.g., [6])

$$\theta = \frac{\cot^{-1}\xi}{\cot^{-1}\xi_0} = \frac{\cot^{-1}\xi}{\cos^{-1}\varepsilon}. \tag{12}$$

The eigenfunction P_m has the following orthogonality property:

$$\int_{-1}^{1} P_m(x)\, P_n(x)\, \mathrm{d}x = \begin{cases} 2/(2m+1) & \text{if} \quad n = m \\ 0 & \text{if} \quad n \neq m \end{cases}, \tag{13}$$

where n is an integer. Using this feature, the unknown coefficients are obtained as

$$A_m = \frac{i}{Q'_m(i\xi_0)}\frac{2m+1}{2(1+\xi_0^2)}\int_{-1}^{1} P_m(\eta)\sqrt{\xi_0^2+\eta^2}\,\mathrm{d}\eta. \tag{14}$$

The integral in Eq. (14) is zero for odd values of m and is otherwise calculated via [7]

$$\int_{-1}^{1} P_m(\eta)\sqrt{\xi_0^2+\eta^2}\,\mathrm{d}\eta = 2^m\sum_{n=0}^{m/2}\frac{\Gamma(m/2+n+1/2)I_{2n}(\xi_0)}{\Gamma(2n+1)\Gamma(m-2n+1)\Gamma(n-m/2+1/2)}, \tag{15}$$

where Γ is the gamma function and

$$\begin{aligned} I_{2n}(\xi_0) &= \int_{-1}^{1}\eta^{2n}\sqrt{\xi_0^2+\eta^2}\,\mathrm{d}\eta \\ &= \frac{2\xi_0}{2n+1}\,{}_2\mathrm{F}_1(-1/2, n+1/2; n+3/2; -\xi_0^{-2}). \end{aligned} \tag{16}$$

Here, ${}_2\mathrm{F}_1$ is the hypergeometric function [5]. Having determined the temperature distribution, the average θ on the surface of the spheroid can be calculated as

$$\begin{aligned} \bar{\theta}_s &= \frac{1}{\mathbb{S}_o}\int_{S_o}\theta\,\mathrm{d}S = \frac{2\pi c^2}{\mathbb{S}_o}\sqrt{1+\xi_0^2}\int_{-1}^{1}\theta\sqrt{\xi_0^2+\eta^2}\,\mathrm{d}\eta \\ &= -\frac{4\pi\sqrt{1+\xi_0^2}}{\mathbb{S}_o}\sum_{m=0}^{\infty}\frac{{A_m}^2}{2m+1}\, iQ'_m(i\xi_0)\, Q_m(i\xi_0), \end{aligned} \tag{17}$$

where

$$\mathbb{S}_o = \int_{S_o} 1\,\mathrm{d}S = 2\pi\left(1+\frac{\xi_0^2}{\sqrt{1+\xi_0^2}}\coth^{-1}\sqrt{1+\xi_0^2}\right). \tag{18}$$

It is worth noting that the results of this section for an oblate spheroid can be converted to those for a prolate spheroid by allowing ε to be greater than one and by replacing ξ with $-i\xi$ in all relations (see, e.g., [8]).

2.2. Temperature field around two identical spheres

Consider a pair of identical spheres, with radius ℓ, that are placed distance $2\ell/\epsilon$ apart, where $0 < \epsilon < 1$. Recall the Cartesian coordinate system of §2.1. Only this time, the origin is located in the middle of the line that connects the center of the spheres and the z axis is oriented in the direction of that line. The natural coordinate system for dealing with this geometry is a bispherical coordinate system (ζ, β, φ) defined as [3,4]

$$x/\cos\varphi = y/\sin\varphi = \frac{\mathrm{c}\sin\beta}{\cosh\zeta-\cos\beta}, \quad z = \frac{\mathrm{c}\sinh\zeta}{\cosh\zeta-\cos\beta}, \tag{19}$$

where $\mathrm{c} = \sqrt{\epsilon^{-2}-1}$ is half the (dimensionless) focal distance and

$$-\infty < \zeta < \infty, \quad 0 \leqslant \beta \leqslant \pi, \quad 0 \leqslant \varphi < 2\pi. \tag{20}$$

The coordinates have the following scale factors:

$$h_\zeta = h_\beta = \frac{\mathrm{c}}{\cosh\zeta-\cos\beta}, \quad h_\varphi = \rho = \frac{\mathrm{c}\sin\beta}{\cosh\zeta-\cos\beta}. \tag{21}$$

Fig. 2 depicts the surfaces of constant ζ and β that are non-intersecting spheres surrounding the foci (points located at $z = \pm\mathrm{c}$) and intersecting tori passing through the focal points, respectively. In this curvilinear coordinate system, the thermally active spheres are represented by $\zeta = \pm\zeta_0 = \cosh^{-1}\epsilon^{-1}$ and $(\zeta, \beta) \to (0, 0)$ correspond to $\tilde{r} \to \infty$.

The boundary-value problem introduced at the beginning of this section can be written in terms of (ζ, β, φ) as [3,4]

$$\begin{aligned} \nabla^2\theta = \frac{(\cosh\zeta-\cos\beta)^3}{c^2\sin\beta}\Bigg[&\frac{\partial}{\partial\zeta}\left(\frac{\sin\beta}{\cosh\zeta-\cos\beta}\frac{\partial\theta}{\partial\zeta}\right)+\frac{\partial}{\partial\beta}\left(\frac{\sin\beta}{\cosh\zeta-\cos\beta}\frac{\partial\theta}{\partial\beta}\right) \\ &+\frac{1}{\sin\beta(\cosh\zeta-\cos\beta)}\frac{\partial^2\theta}{\partial\varphi^2}\Bigg] = 0 \\ \text{with}\ \ &\frac{1}{h_\zeta}\frac{\partial\theta}{\partial\zeta}\bigg|_{\zeta=\pm\zeta_0} = \pm 1 \ \ \text{and} \ \ \theta \to 0 \ \text{as} \ (\zeta,\beta)\to(0,0). \end{aligned} \tag{22}$$

The boundary conditions are, again, independent of φ, which simplifies Laplace's equation to

$$\frac{\partial}{\partial\zeta}\left(\frac{\sin\beta}{\cosh\zeta-\cos\beta}\frac{\partial\theta}{\partial\zeta}\right)+\frac{\partial}{\partial\beta}\left(\frac{\sin\beta}{\cosh\zeta-\cos\beta}\frac{\partial\theta}{\partial\beta}\right) = 0. \tag{23}$$

Unlike Eq. (8), this equation is not *simply separable* and belongs to a class of partial differential equations called *R-separable* equations [4]. Therefore, to solve Eq. (23), we start with the ansatz $\theta(\zeta,\beta) = \sqrt{\cosh\zeta-\cos\beta}\,\mathcal{Z}(\zeta)\,\mathcal{B}(\beta)$, where $\mathcal{Z}$ and $\mathcal{B}$ are the unknown functions we seek to determine. Substituting the proposed form for θ into Eq. (23), we arrive at a pair of ordinary differential equations for $\mathcal{Z}$ and $\mathcal{B}$. Upon solving those equations, the following general solution for θ emerges [3,4]:

$$\begin{aligned} \theta = \sqrt{\cosh\zeta-\cos\beta}\sum_{m=0}^{\infty}&\Big[B_m^1\sinh(m+1/2)\zeta + B_m^2\cosh(m+1/2)\zeta\Big] \\ &\times\Big[B_m^3 P_m(\cos\beta) + B_m^4 Q_m(\cos\beta)\Big], \end{aligned} \tag{24}$$

where $B_m^1, \ldots, B_m^4$ are constant coefficients.

As indicated before, the function $Q_m(\cos\beta)$ is singular at $\cos\beta = \pm 1$. Thus, B_m^4 vanish in order to retain the regularity of the solution. One can infer from the geometry of the problem and the boundary conditions that the temperature distribution is symmetric about the $x-y$ plane, which means $\partial\theta/\partial\zeta = 0$ at $\zeta = 0$. To satisfy this condition, we must set $B_m^1 = 0$. Conveniently, the infinity boundary condition is already satisfied thanks to the term outside the summation that approaches zero as $(\zeta,\beta)\to(0,0)$. Incorporating these results, the solution for θ reduces to

$$\theta = \sqrt{\cosh\zeta-\cos\beta}\sum_{m=0}^{\infty} B_m\cosh(m+1/2)\zeta\, P_m(\cos\beta), \tag{25}$$

where the constant coefficients B_m are determined by enforcing the normal gradient boundary condition on the surface of the spheres, i.e.,

$$\begin{aligned} \frac{1}{h_\zeta}\frac{\partial\theta}{\partial\zeta}\bigg|_{\zeta=\zeta_0} = -\frac{1}{h_\zeta}\frac{\partial\theta}{\partial\zeta}\bigg|_{\zeta=-\zeta_0} &= \frac{\sqrt{\cosh\zeta_0-\cos\beta}}{c} \\ &\times\sum_{m=0}^{\infty} B_m[D_m P_m(\cos\beta) - E_m\cos\beta P_m(\cos\beta)] = 1, \end{aligned} \tag{26}$$

where

$$D_m = \frac{\sinh\zeta_0\cosh(m+1/2)\zeta_0}{2} + (m+1/2)\cosh\zeta_0\sinh(m+1/2)\zeta_0,$$
$$E_m = (m+1/2)\sinh(m+1/2)\zeta_0. \tag{27}$$

Yet, again, we see that the application of the constant flux boundary condition results in a more convoluted equation for the unknown coefficients compared to the situation where the isothermal condition $\theta = 1$ is imposed at $\zeta = \pm\zeta_0$ (see, e.g., [9]).

In addition to the orthogonality property Eq. (13), the following integral relations apply to the eigenfunction P_m [7]:

$$\int_{-1}^{1} P_m(x)\,P_n(x)\,x\,\mathrm{d}x = \begin{cases} \frac{2(m+1)}{(2m+1)(2m+3)} & \text{if} \quad n = m+1 \\ \frac{2m}{(2m-1)(2m+1)} & \text{if} \quad n = m-1 \\ 0 & \text{if} \quad n \neq m \pm 1 \end{cases},$$
$$\int_{-1}^{1} \frac{P_m(x)}{\sqrt{\cosh\zeta_0 + x}}\,\mathrm{d}x = \frac{2\sqrt{2}}{2m+1}\,e^{-(m+1/2)\zeta_0}. \tag{28}$$

Utilizing the above relations in conjunction with Eq. (13), we obtain a recursive formula for the coefficients in the form of

$$B_1 = F_0 + B_0,$$
$$B_{m+1} = F_m + G_m B_m + (1 - G_m)B_{m-1}, \tag{29}$$

where

$$F_m = -\frac{2\sqrt{2}\,\sinh\zeta_0\,e^{-(m+1/2)\zeta_0}}{(m+1)\sinh(m+3/2)\zeta_0},$$
$$G_m = \frac{1}{m+1}\left[1 + \frac{2m\cosh\zeta_0\sinh(m+1/2)\zeta_0}{\sinh(m+3/2)\zeta_0}\right]. \tag{30}$$

We are now left with the task of determining B_0, accomplished by demanding the terms in the solution that correspond to large eigenvalues to be finite. This condition is satisfied by requiring $B_m \to 0$ as $m \to \infty$, which, after some mathematical manipulations, yields

$$B_0 = -\lim_{m\to\infty} H_m, \tag{31}$$

where

$$H_0 = F_0, \quad H_1 = F_1 + G_1 F_0,$$
$$H_m = F_m + G_m H_{m-1} + (1 - G_m)H_{m-2}. \tag{32}$$

With the coefficients known, the mean θ over the surface of each sphere is calculated via

$$\bar{\theta}_s = \frac{1}{\mathbb{S}_o}\int_{S_o}\theta\,\mathrm{d}S = \frac{2\pi c^2}{\mathbb{S}_o}\int_0^{\pi}\frac{\theta\sin\beta}{(\cosh\zeta_0 - \cos\beta)^2}\,\mathrm{d}\beta$$
$$= \frac{\sinh\zeta_0}{\sqrt{2}}\sum_{m=0}^{\infty} B_m\left[1 + e^{-(2m+1)\zeta_0}\right]. \tag{33}$$

3. Results and discussion

We begin with the results for oblate spheroids. First, we consider the limiting cases of $\varepsilon = 1$ (sphere) and $\varepsilon = 0$ (disk). The results for the former have been already known to be

$$\theta = 1/\tilde{r}, \quad \bar{\theta}_s = 1, \quad \mathrm{Nu} = 2. \tag{34}$$

For the latter, however, we find

$$A_m = \begin{cases} \frac{i(2m+1)}{(m-1)(m+2)}\left\{\frac{m!}{2^m[(m/2)!]^2}\right\}^2 & \text{if} \quad m \equiv 0\,(\mathrm{mod}2) \\ 0 & \text{if} \quad m \equiv 1\,(\mathrm{mod}2) \end{cases}, \tag{35}$$

which, consistent with [1], results in

$$\bar{\theta}_s = 8/3\pi, \quad \mathrm{Nu} = 3\pi/8. \tag{36}$$

Next, we examine other aspect ratios. Quite unexpectedly, our calculations indicate that the series solution for the temperature (see Eq. (10)) is very well approximated by its first two non-zero terms for the entire range of ε, i.e.,

$$\theta \approx \sqrt{1+\xi_0^2}\left\{\frac{\mathbb{S}_o}{4\pi}\cot^{-1}\xi + \frac{5}{64}\left[(2+3\xi_0^2) + (4+3\xi_0^2)\left(1 - \frac{\mathbb{S}_o}{2\pi}\right)\right]\right.$$
$$\left.\times\left[\frac{3\xi - (3\xi^2+1)\cot^{-1}\xi}{3(1+\xi_0^2)\xi_0\cot^{-1}\xi_0 - (2+3\xi_0^2)}\right](3\eta^2 - 1)\right\}. \tag{37}$$

In fact, the maximum percent difference between the results corresponding to $m = 3$ and $m = 19$ happens to be less than 4%. A visually convincing demonstration of this result is provided in Fig. 3, where we present side-by-side contour plots of the temperature field (in meridian planes) around an oblate spheroid of aspect ratio $\varepsilon = 0.3$. As you can see, the approximate results of Fig. 3a are barely distinguishable from the (nearly) exact results of Fig. 3b.

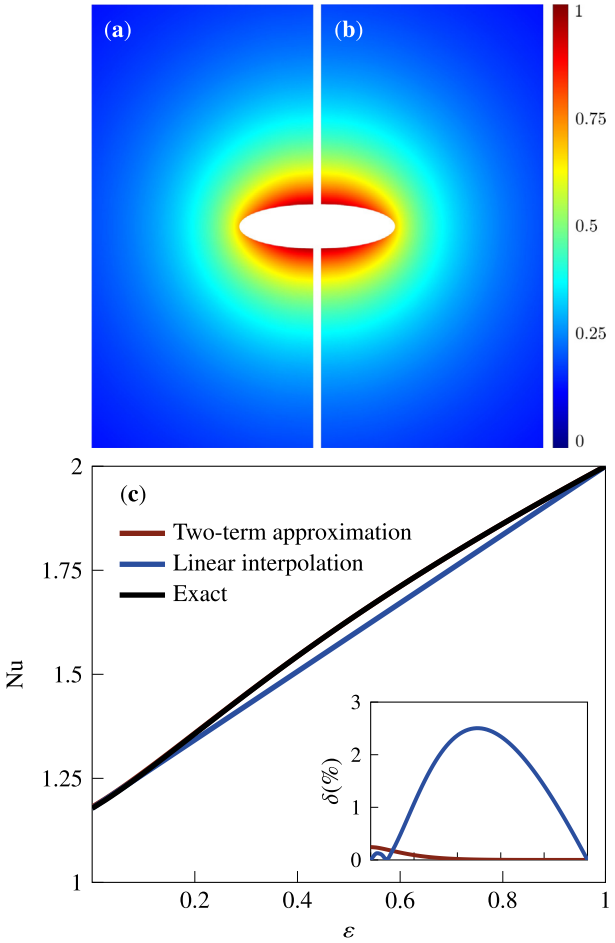

Fig. 3. (a) and (b) Contour plots of the (dimensionless) temperature field θ (in meridian planes) around an oblate spheroid of aspect ratio $\varepsilon = 0.3$. The left panel illustrates the results of the two-term approximation whereas the right panel presents those obtained by setting $m = 19$, considered here as exact results. (c) The Nusselt number Nu versus the aspect ratio ε for oblate spheroids. Red, blue, and black lines represent the results corresponding to $m = 3$, linear interpolation based on the Nu of sphere and disk, and $m = 19$, respectively. The inset shows the relative difference between the approximate and exact results. (For interpretation of the references to colour in this figure legend, the reader is referred to the web version of this article.)

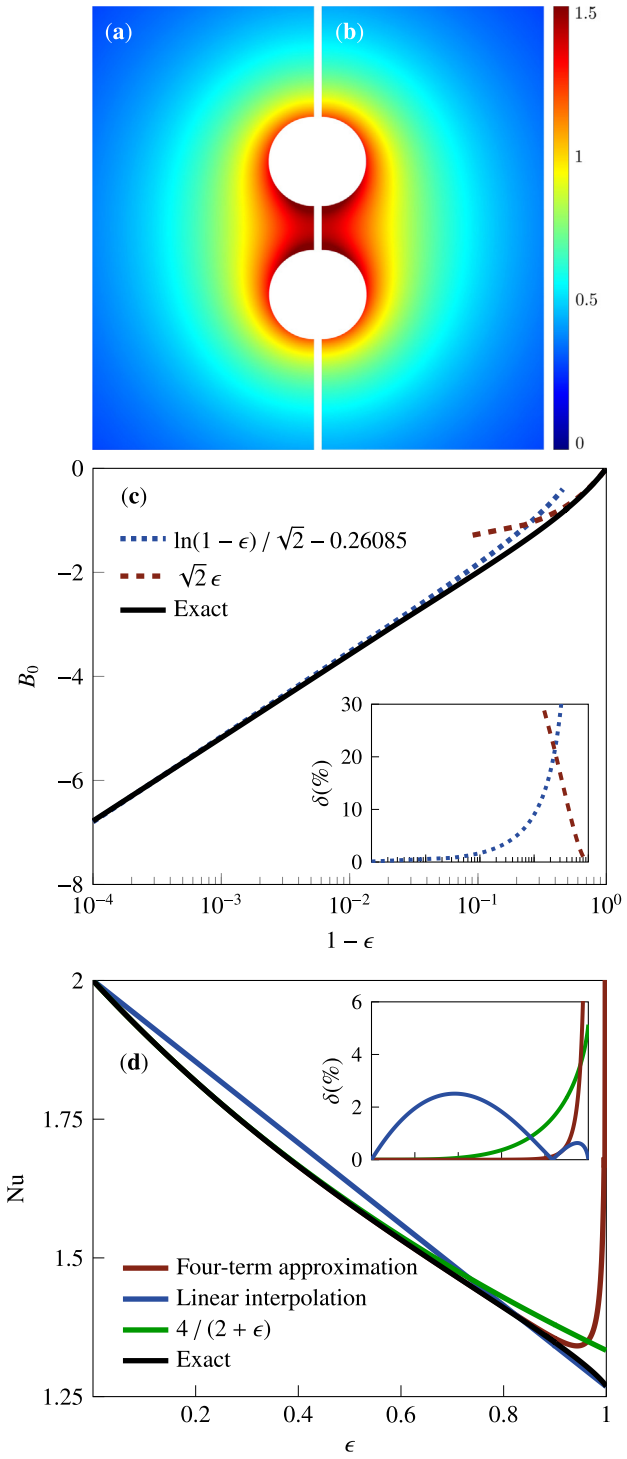

Fig. 4. (a) and (b) Contour plots of the (dimensionless) temperature field θ (in meridian planes) around two spheres whose centers are three radii apart ($\epsilon = 2/3$). The left panel illustrates the results of the four-term approximation whereas the right panel presents those obtained by setting $m = 9$, considered here as exact results. (c) B_0 as a function of $1 - \epsilon$, where the dashed and dotted lines represent the asymptotic approximations in the limits of $\epsilon \to 0$ and $\epsilon \to 1$, respectively. And, the inset shows the relative error of the approximations. (d) The Nusselt number Nu versus the inverse of the dimensionless separation distance ϵ for a pair of identical spheres. Red, blue, green, and black lines represent the results corresponding to $m = 3$, linear interpolation based on the Nu of single sphere and two touching spheres, asymptotic behavior in the limit of $\epsilon \to 0$, and the converged solution (i.e., $m \gg 1$), respectively. The inset shows the relative difference between the approximate and exact results. (For interpretation of the references to colour in this figure legend, the reader is referred to the web version of this article.)

Equally interesting, we also find that the average Nusselt number for oblate spheroids varies almost linearly with the aspect ratio (see Fig. 3c). Therefore, the Nu versus ε curve can be approximated by the line that passes through its end points, i.e.,

$$\mathrm{Nu} \approx \mathrm{Nu}_{\mathrm{disk}} + (\mathrm{Nu}_{\mathrm{sphere}} - \mathrm{Nu}_{\mathrm{disk}})\varepsilon = \frac{3\pi}{8} + \left(2 - \frac{3\pi}{8}\right)\varepsilon. \tag{38}$$

The maximum relative error of this approximation occurs at $\varepsilon \approx 0.5$ and falls below 3%, which underscores its validity for all aspect ratios (see the inset of Fig. 3c). Furthermore, from Fig. 3c and its inset, we learn that the Nusselt number calculated based on the two-term representation of θ is extremely accurate, differing less than 0.25% from the actual values.

We now analyze the results for bispheres. In the limit $\epsilon \to 0$, the spheres are very far from each other and, therefore, the solution simplifies to Eq. (34) for a single sphere. On the other hand, when $\epsilon \to 1$ (i.e., when the gap between the spheres vanish), Eq. (25) for the temperature distribution does not immediately reduce to a simple form. The average surface temperature and Nusselt number in this case are $\bar{\theta}_s = 1.57721$ and $\mathrm{Nu} = 1.26806$.

Again, we observe that setting $m = 3$ in the series solution for θ (Eq. (25)) provides excellent results, accurate to within 5% of the converged solution for $0 < \epsilon < 4/5$ (see, e.g., Fig. 4a and b). As the gap between the spheres narrows, the error of the four-term approximation increases, which means that more terms are needed to represent the temperature field accurately. For example, the error grows to 10% as the gap size reduces to $\ell/4$.

Given the recursive relation defined in Eq. (29), what carries the most weight in calculating B_m is determining B_0. Fig. 4c shows the variation of this coefficient as a function of $1 - \epsilon$. As it can be seen, B_0 approaches zero as $\sqrt{2}\epsilon$ when the distance between the spheres is large and it asymptotes to $-\infty$ as $\ln(1-\epsilon)/\sqrt{2} - 0.26085$ when the spheres almost touch each other. The asymptotic formulas can be used to estimate, with reasonable accuracy, the value of B_0 over a wide range of ϵ (see the inset of Fig. 4c).

Lastly, our calculations indicate that the Nusselt number of the two-sphere system, like that of the oblate spheroid changes almost linearly with ϵ (see Fig. 4d). Hence, again, a linear interpolation using the Nu of a single sphere and a pair of touching spheres can be employed to effectively approximate the curve of Nu versus ϵ (see the inset of Fig. 4d). There exists another approach for approximating this curve based on the asymptotic behavior of $\bar{\theta}_s$ in the limit $\epsilon \to 0$. When the spheres are widely separated, they see each other as a point source/sink. Thus, to the leading order in ϵ, the average surface temperature and consequently the Nusselt number take the forms of $\bar{\theta}_s = 1 + \epsilon/2$ and $\mathrm{Nu} = 4/(2+\epsilon)$. Perhaps surprisingly, this approximation outperforms the linear interpolation for gap sizes larger than the radius of the spheres (compare blue and green lines in the inset of Fig. 4d).

4. Summary

We derived analytical solutions for the problems of conduction heat transfer from an isolated oblate spheroid and a pair of spheres. The derivations were carried out in curvilinear coordinate systems, befitting each geometry, using the method of separation of variables and eigenfunction expansion. While the solutions are in the form of infinite series, we showed that considering only the first few terms provides excellent results, often accurate to within a few percent of the exact values. We also found that the Nusselt number in both cases considered varies rather linearly with respect to the relevant dimensionless length scale of the problem. Needless to say, these and other findings of this study apply

equally well to equivalent mass transfer problems. Furthermore, our results can be used to develop perturbation solutions for the problems of forced convection heat transfer from heated spheroids and bispheres in uniform laminar flows at small Péclet numbers [10–12].

In conclusion, it is worth noting that although there have been many studies on analytical modeling of conduction heat transfer from objects of various shapes (or analogous problems in mass transfer, electrostatics, etc.), a large number of them have focused on the isothermal (Dirichlet) boundary condition (see, e.g., [6,9,13–22]) and a relatively small number have considered the uniform flux (Neumann) boundary condition (see, e.g., [11,23]). Here, we have attempted to partially fill this gap in the literature. However, still many problems in this area remain unexplored.

Conflict of interest

The authors declare no conflict of interest.

Acknowledgement

Partial support from the National Science Foundation under Grant No. CBET-1749634 is acknowledged. This research was carried out in part using the computational resources provided by the Superior high-performance computing facility at Michigan Technological University.

References

[1] F.P. Incropera, A.S. Lavine, T.L. Bergman, D.P. DeWitt, Fundamentals of Heat and Mass Transfer, Wiley, New York, 2011.
[2] F. Moukalled, L. Mangani, M. Darwish, The Finite Volume Method in Computational Fluid Dynamics: An Advanced Introduction with OpenFOAM® and Matlab®, vol. 113, Springer, 2015.
[3] P.M. Morse, H. Feshbach, Methods of Theoretical Physics, McGraw-Hill, New York, 1953.
[4] P. Moon, D.E. Spencer, Field Theory Handbook: Including Coordinate Systems, Differential Equations and Their Solutions, Springer-Verlag, New York, 1988.
[5] M. Abramowitz, I.A. Stegun, Handbook of Mathematical Functions: With Formulas, Graphs, and Mathematical Tables, Dover, New York, 1972.
[6] R.S. Alassar, Heat conduction from spheroids, J. Heat Transfer 121 (1999) 497–499.
[7] I.S. Gradshteyn, I.M. Ryzhik, Table of Integrals, Series, and Products, Academic Press, Boston, 2007.
[8] J. Happel, H. Brenner, Low Reynolds Number Hydrodynamics, with Special Applications to Particulate Media, Martinus Nijhoff, The Hague, The Netherlands, 1983.
[9] R.S. Alassar, B.J. Alminshawy, Heat conduction from two spheres, AIChE J. 56 (2010) 2248–2256.
[10] L.G. Leal, Advanced Transport Phenomena: Fluid Mechanics and Convective Transport Processes, Cambridge University Press, Cambridge, 2007.
[11] L.A. Romero, Low or high Péclet number flow past a prolate spheroid in a saturated porous medium, SIAM J. Appl. Math. 55 (1995) 952–974.
[12] E. Dehdashti, H. Masoud, Forced convection heat transfer from a particle at small and large Péclet numbers, Int. J. Heat Mass Transfer (2019), submitted for publication.
[13] J.E. Sunderland, K.R. Johnson, Shape factors for heat conduction through bodies with isothermal or convective boundary conditions, ASHRAE Trans. 70 (1964) 237–241.
[14] M.M. Yovanovich, A general expression for predicting conduction shape factors, in: Thermophysics and Spacecraft Thermal Control, American Institute of Aeronautics and Astronautics, 1974, pp. 265–291.
[15] E. Hahne, U. Grigull, Shape factor and shape resistance for steady multidimensional heat conduction, Int. J. Heat Mass Transfer 18 (1975) 751–767.
[16] H. Brenner, S. Haber, Symbolic operator solutions of Laplace's and Stokes' equations: Part I Laplace's equation, Chem. Eng. Commun. 27 (1984) 283–295.
[17] W.M. Rohsenow, J.P. Hartnett, Y.I. Cho, Handbook of Heat Transfer, McGraw-Hill, New York, 1998.
[18] H. Le-Quang, G. Bonnet, Q.-C. He, Size-dependent Eshelby tensor fields and effective conductivity of composites made of anisotropic phases with highly conducting imperfect interfaces, Phys. Rev. B 81 (2010) 064203.
[19] R.S. Alassar, Conduction in eccentric spherical annuli, Int. J. Heat Mass Transfer 54 (2011) 3796–3800.
[20] A. Yılmazer, C. Kocar, Exact solution of the heat conduction equation in eccentric spherical annuli, Int. J. Therm. Sci. 68 (2013) 158–172.
[21] R. Shah, T. Li, The thermal and laminar boundary layer flow over prolate and oblate spheroids, Int. J. Heat Mass Transfer 121 (2018) 607–619.
[22] S. Lee, J. Lee, B. Ryu, S. Ryu, A micromechanics-based analytical solution for the effective thermal conductivity of composites with orthotropic matrices and interfacial thermal resistance, Sci. Rep. 8 (2018) 7266.
[23] Y. Solomentsev, D. Velegol, J.L. Anderson, Conduction in the small gap between two spheres, Phys. Fluids 9 (1997) 1209–1217.